The Sixteenth International Congress on Sound and Vibration
Kraków, 5-9 July 2009

ON THE USE OF NEAR-FIELD ACOUSTICAL HOLOGRAPHY TO STUDY THE TRANSIENT RADIATION OF IMPACTED PLATES

Jean-François Blais

Bombardier Aerospace, 400 Côte-Vertu Road West, Dorval (Québec), Canada, H4S 1Y9

Annie Ross

CREPEC, Department of Mechanical Engineering, École Polytechnique de Montréal, CP 6079 station Centre-ville, Montréal (Québec), Canada, H3C 3A7
Email address: annie.ross@polymtl.ca

This paper discusses the application of near-field acoustical holography to visualize the sound pressure radiated by impacted plates as a function of time. It is known that when Fourier transform based near-field acoustical holography is applied to propagate sound fields away from the acoustic source, the use of direct and inverse time domain discrete Fourier transforms leads to significant aliasing errors in the reconstructed time signals. To avoid such errors, the time domain discrete Fourier transform can be replaced by a numerical Laplace transform as long as the Dirichlet k-space Green's function is reformulated. In the present paper, the resulting transient acoustical holography method is applied experimentally to study the sound radiation of a free plexiglas plate impacted at its center by a steel pendulum. Forward propagated signals show good agreement with measured signals in propagation planes at distances up to 20 cm from the hologram, i.e. distances comparable to the plate dimensions. A time and space reconstruction of the sound pressure field is also computed from the measured hologram. Both airborne and structure-borne sound radiation can be observed as a function of time in a plane perpendicular to the plate. For instance, sound pressure wavefronts due to the reflection of flexural waves on the edges of the plate are clearly visible in this reconstruction.

1. Introduction

Noise produced by impacted structures in industrial applications such as riveting and hammering can cause hearing impairment. In these sound fields, transient phenomena such as the radiation due to the reflection of flexural waves in the structure (at edges, holes or any local changes in the structure's mechanical impedance) have time and space properties which are of interest for the development of impact noise control devices [1]. Accordingly, a time and space visualization technique such as near-field acoustical holography (NAH) [2] could be used as a tool to gain a better understanding of these transient acoustic phenomena and thus, lead to better control devices.

It is known that when Fourier transform based NAH is applied to propagate sound fields away from an acoustic source, the use of direct and inverse time domain discrete Fourier transforms (DFTs) leads to significant aliasing errors in the reconstructed time signals [3]. Such errors can be reduced by

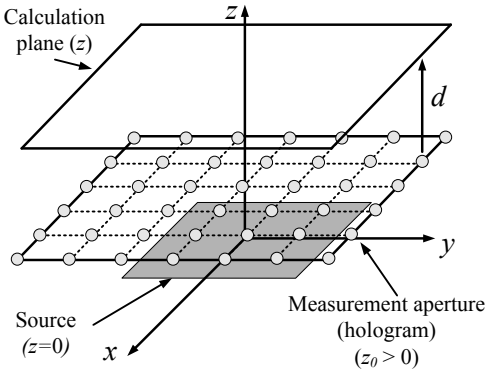

Figure 1. Overview of planar TNAH.

adding trailing zeros to initial time signals. However, this approach results in considerable computing requirements. This issue can be overcome with the transient NAH (TNAH) formulation introduced by Blais and Ross [4]. This method suppresses time aliasing errors without requiring zero padding since time domain DFTs are replaced by numerical Laplace transforms (NLTs). The Dirichlet k-space Green's function is also reformulated.

In the present paper, application of TNAH for time and space reconstruction of transient sound pressure fields is discussed. It is proposed to study the sound radiated by a free Plexiglas plate impacted by a steel pendulum. The basics of the TNAH formulation and the experimental setup are presented first. Phenomena observable in the measured hologram are described. Forward propagated signals obtained with TNAH are then compared to measured signals in projection planes. Finally, a time and space reconstruction, which is computed with several forward propagations, is discussed.

2. Transient near-field acoustical holography

Since the Laplace transform is a common tool to study transient phenomena, it is appropriate to use it with respect to the time variable of pressure fields. Let us first consider the angular spectrum $P(k_x, k_y, z, s)$ of a given sound pressure field $p(x, y, z, t)$, where k_x and k_y are the trace wavenumbers in the x and y directions (Fig. 1), and s is the complex Laplace variable. The angular spectrum is obtained by combining a Laplace transform in the time domain and a two-dimensional Fourier transform in the space domain, i.e.

$$P(k_x, k_y, z, s) = \int_0^{+\infty} \iint_{-\infty}^{+\infty} p(x, y, z, t) e^{-i(k_x x + k_y y) + st} dx\, dy\, dt. \tag{1}$$

The inverse transforms are written as

$$p(x, y, z, t) = \frac{1}{8i\pi^3} \int_{\sigma - i\infty}^{\sigma + i\infty} \iint_{-\infty}^{+\infty} P(k_x, k_y, z, s) e^{i(k_x x + k_y y) - st} dk_x\, dk_y\, ds, \tag{2}$$

where $s = \sigma + i\omega$ and ω is the angular frequency. According to the definition of the Laplace transform, the artificial damping factor σ is negative to ensure convergence of the time integral in Eq. (1).

As in the Fourier transform based NAH formulation, the sound pressure field measured in a given plane z_0 shown in Fig. 1 can be propagated to any plane $z \geq 0$ by applying a k-space Dirichlet Green's function to the angular spectrum, i.e. [4]

$$P(k_x, k_y, z, s) = P(k_x, k_y, z_0, s) e^{ik_z d}, \tag{3}$$

where

$$k_z^2 = -\left(k_x^2 + k_y^2 + \frac{s^2}{c^2}\right) \text{ and } d = z - z_0.$$

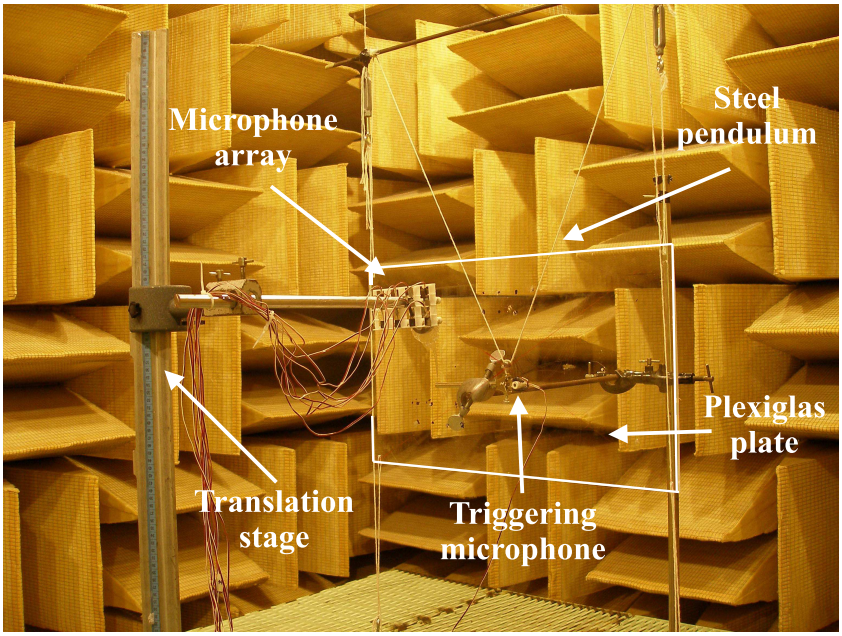

Figure 2. Experimental setup.

The sound velocity in the ambient medium is noted c. One could notice that when $\sigma = 0$, Eqs. (1) to (3) are the same as those defined in the Fourier transform based NAH formulation [2].

With appropriate variable changes, direct and inverse Laplace transforms can be defined in terms of Fourier transforms and hence, can be computed numerically through fast Fourier transform (FFT) algorithms. The resulting algorithms are known as the direct and inverse numerical Laplace transforms [5]. Consequently, Eqs. (1) and (2) can be written as

$$P(k_x, k_y, z, s) = \mathscr{F}_{xy}\left\{\mathscr{F}_t\left\{p(x, y, z, t)e^{\sigma t}\right\}\left[\Lambda(x)\Lambda(y)\right]^{1/2}\right\} \tag{4}$$

and

$$p(x, y, z, t) = e^{-\sigma t}\mathscr{F}_t^{-1}\left\{\mathscr{F}_{xy}^{-1}\left\{P(k_x, k_y, z, s)\right\}\Lambda(\omega)\right\}, \tag{5}$$

where $\mathscr{F}$ and $\mathscr{F}^{-1}$ are respectively the direct and inverse FFTs in the space (subscript xy) and time (subscript t) domains. Tukey windows are also applied in both space and frequency domains. They are defined as

$$\Lambda(\xi) = \begin{cases} 1 & |\xi| < \xi_m - \xi_w \\ \frac{1}{2}\left[1 - \cos\left(\frac{\pi(|\xi| - \xi_m)}{\xi_w}\right)\right] & \xi_m - \xi_w \leq |\xi| \leq \xi_m \end{cases} \tag{6}$$

where ξ_m is the maximum value taken by ξ (corresponding to x, y or ω), and ξ_w is the width of the tapered rim. A spatial window is used in Eq. (4) to reduce spectral leakage due to the truncation of the measurement aperture. A similar window is applied in the frequency domain to avoid amplification of the Gibbs phenomenon caused by the exponential term in Eq. (5) [6]. Nevertheless, even with frequency windowing, a large value of σ, which suppresses time aliasing, can still amplify the Gibbs phenomenon. Wedepohl [7] proposed a suitable trade-off by setting the artificial damping factor to $\sigma = -2\ln(N_t)/T$, where N_t is the number of points in time signals of duration T.

3. Experimental setup

The experimental setup in Fig. 2 was used in an anechoic chamber to study the sound radiated by an impacted plate. A Plexiglas plate of dimensions $L_x \times L_y = 50.6 \times 29.4$ cm^2 and thickness

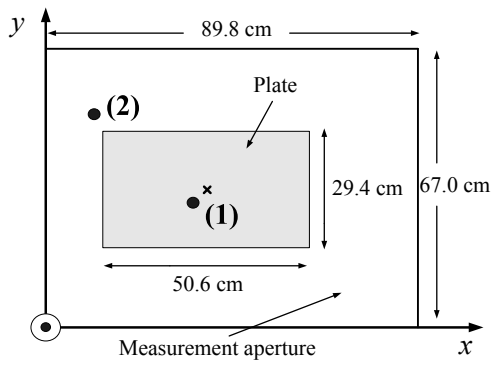

Figure 3. Measurement aperture size as compared to plate size. Experimental validation was performed at points (1) and (2). The cross (×) indicates the impact location.

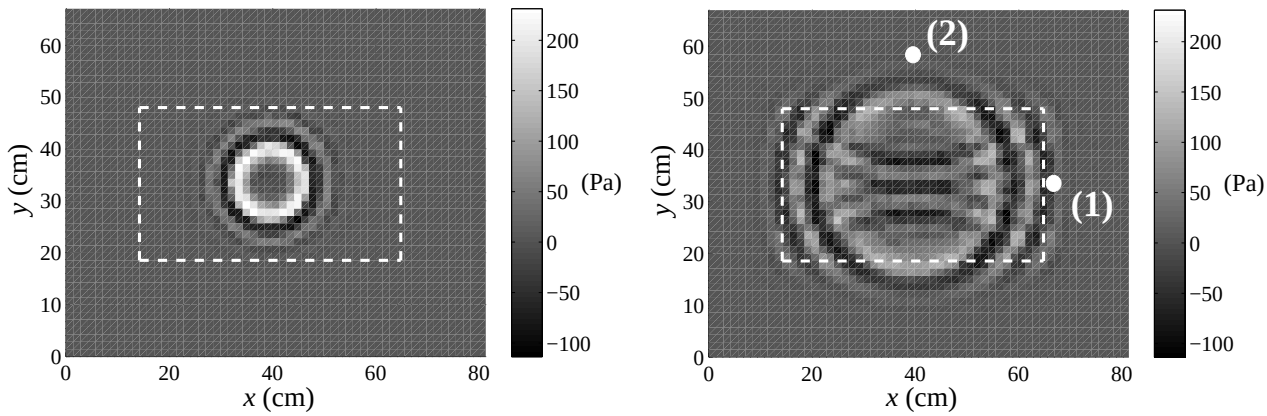

(a) $t = 0.21$ ms **(b)** $t = 0.48$ ms

Figure 4. Instantaneous sound pressure in the hologram plane at two different times t after the beginning of the impact. The dashed white rectangle illustrates the plate location with respect to the measurement aperture.

$h = 5.8$ mm was hung at its four corners. It was impacted at its center by a steel pendulum of radius $r_s = 5.5$ mm at a velocity $v_s = 2$ m/s.

A 2-axes manual translation stage was used to displace the 4 by 2 microphone array. The 130A Acousticel electret microphones were calibrated in amplitude and phase. They were connected to a NI PXI-4472 acquisition device. The sampling frequency was set to $F_s = 102.4$ kHz. Acquisition was triggered by another microphone located at 2.3 cm from the impact axis and at 2 cm from the plate.

4. Results

4.1 Measured hologram

The translation stage in Fig. 2 was moved over a plane of dimensions 89.8×67.0 cm^2 shown in Fig. 3 and located at $z_0 = 2$ cm. Measurement points were equally spaced by $\Delta x = \Delta y = 1.4$ cm. Sound pressure time signals were acquired over a duration $T = 2.5$ ms.

Figure 4 shows the instantaneous sound pressure in the hologram plane at two different times after the beginning of the impact. The dashed white rectangle illustrates the plate location with respect to the measurement aperture. In Fig. 4(a) the circular symmetry of the sound radiation is clearly visible even though the plate is rectangular. This can be explained by the fact that at $t = 0.21$ ms,

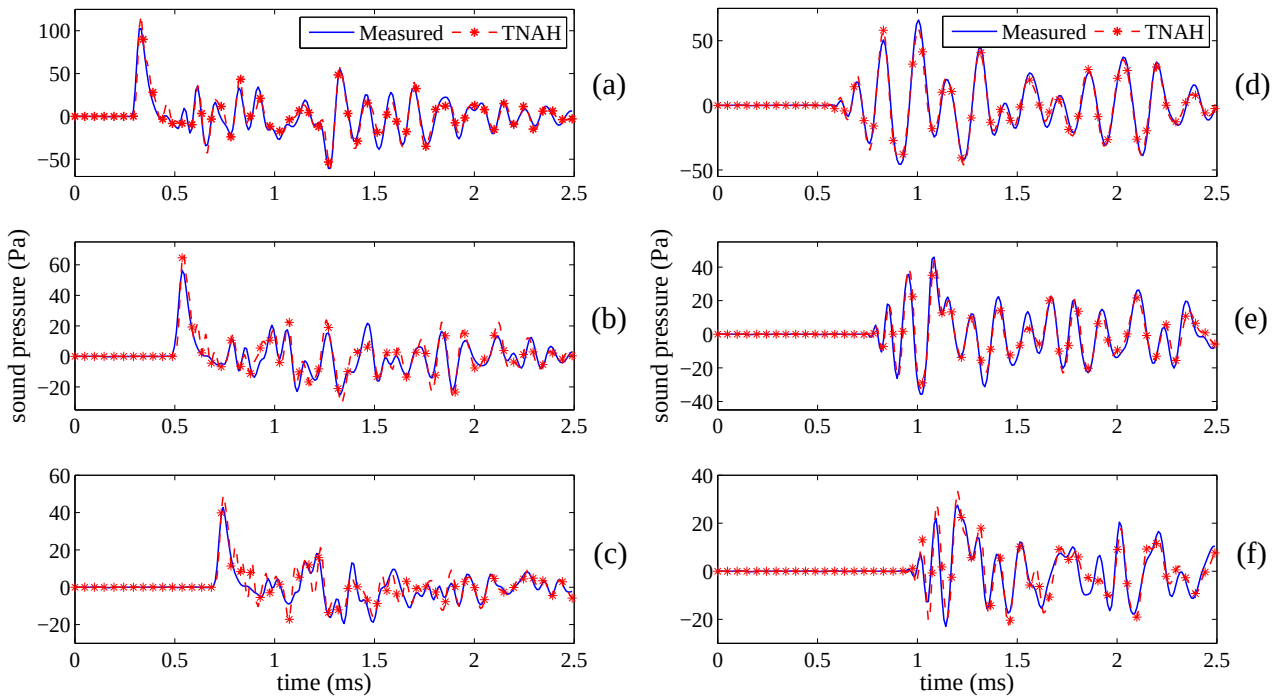

Figure 5. Time signals propagated with TNAH and measured at: (a) point (1) and $z = 9$ cm, (b) point (1) and $z = 16.6$ cm, (c) point (1) and $z = 23.6$ cm, (d) point (2) and $z = 9$ cm, (e) point (2) and $z = 16.6$ cm, (f) point (2) and $z = 23.6$ cm.

the radiation due to the reflection of flexural waves at the edges of the plate have not reached the hologram. The rings visible in Fig. 4(a) are all centered on the impact location.

The rings shown in Fig. 4(b) at $t = 0.48$ ms are larger than those observed in Fig. 4(a). In that case, the rings are not symmetric since they are not entirely over the plate and because the sound pressure decreases as a function of the distance from the plate. For instance, in Fig. 4(b), the sound pressure at point (1) is larger than that at point (2) since point (1) is located closer to the plate. Moreover, the sound radiation due to the reflection of flexural waves at the edges of the plate parallel to the x-axis is clearly visible. The shape of these wavefronts is similar to hyperbolas.

4.2 Validation of forward propagation

The TNAH approach presented in Sec. 2 was applied to the measured hologram by implementing Eqs. (3) to (5) in MATLAB. The width of the tapered rim of the Tukey window defined in Eq. (6) and applied in Eq. (4) was set to $x_w = y_w = 5.7$ cm. The number of points was doubled in each direction with zero padding to avoid spatial wraparound. The bandwidth of the tapered rim of the Tukey window used in the frequency domain in Eq. (5) was chosen as $\omega_w = \pi F_s/2$.

TNAH propagation results were compared to measurements in the projection plane. These time signals are shown in Fig. 5 for two observation points indicated in Fig. 3. Point (1) is located near the impact axis and point (2) is outside the plate area. The time signals are shown in Fig. 5 for three propagation distances: $d = 7$ cm [(a) and (d)], $d = 14.6$ cm [(b) and (e)] and $d = 21.6$ cm [(c) and (f)].

The initial propagation delays of the propagated signals shown in Fig. 5 are in good agreement with measured signals, regardless of the propagation distance or the location of the observation point. Likewise, the time of arrival of each local minima and maxima are quite similar, even at the beginning

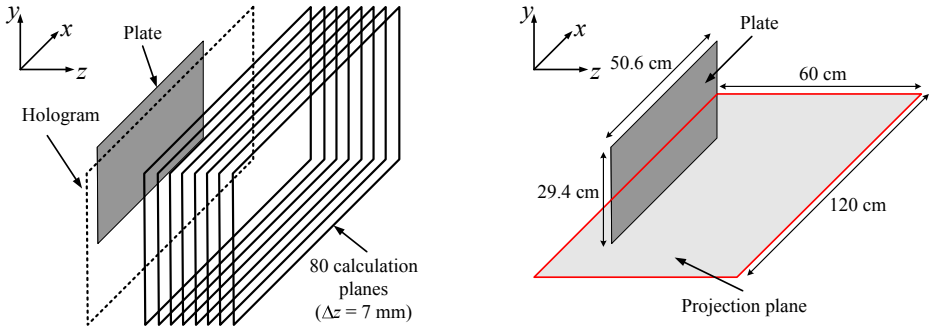

(a) Propagation to several parallel planes. **(b)** Normal projection plane.

Figure 6. Time and space visualization process.

of signals for which the amplitude fluctuates rapidly, such as in Fig. 5(f). The time and amplitude errors are mainly due to the lack of precision of the experimental setup.

4.3 Time and space sound field reconstruction

Since forward propagation was validated for different observation points and propagation distances, TNAH can be used to visualize the sound pressure field as a function of time. Such reconstruction was carried out by propagating the hologram to 80 parallel planes equally spaced by 7 mm as shown in Fig. 6(a). Extra zeros added to extend the measurement aperture were kept in order to enlarge the reconstruction. Finally, a projection plane perpendicular to the y-axis and shown in Fig. 6(b) was chosen for further analysis. This plane is located at 4 mm from the impact location.

Figure 7 shows the spatial reconstruction at three different times t after the beginning of the impact. The plate and the hologram locations are respectively illustrated by solid black and dashed white lines. The sound pressure at $t = 0.38$ ms is shown in Fig. 7(a). A large amplitude hemispherical wavefront due to the local deformation of the plate at the impact location is visible at point (1). Moreover, several oblique wavefronts at different angles are observable at point (2). This phenomenon is known as apparent dispersion [8] and is illustrated in Fig. 8. Due to continuity at the air to plate interface, the acoustic wave trace along the plate travels at the same velocity c_b as the bending wave in the plate. This behavior was also clearly observed by Schedin *et al.* using an optical interferometry technique [1].

At $t = 0.72$ ms in Fig. 7(b), the main hemispherical wavefront at point (1) and oblique wavefronts at point (2) are still visible. Another wavefront due to the reflection of the flexural waves on the two edges of the plate parallel to the x-axis is observable at point (3). Oblique wavefronts are also visible at point (4). They are caused by the radiation of the flexural waves reflected back to the center of the plate on the edges parallel to the y-axis. Finally, phenomena (1) to (4) observed in Fig. 7(b) are still visible in Fig. 7(c) at $t = 1.7$ ms even though the amplitude of the sound pressure is smaller.

5. Conclusion

The application of TNAH to visualize the radiation of an impacted plate was discussed. The sound radiated by a free Plexiglas plate impacted by a steel pendulum was studied. It was shown that the hologram itself provides information about the source. The impact location and the radiation due to the reflection of flexural waves on the edges of the plate can be clearly identified. Forward propagated signals also show good agreement with measured signals in propagation planes at distances up to 20 cm from the hologram, i.e. distances comparable to the plate dimensions. Time of arrivals of the various sound pressure peaks were accurate, regardless of the location of the observation point or the propagation distance. Finally, a time and space reconstruction was computed. Mainly, apparent

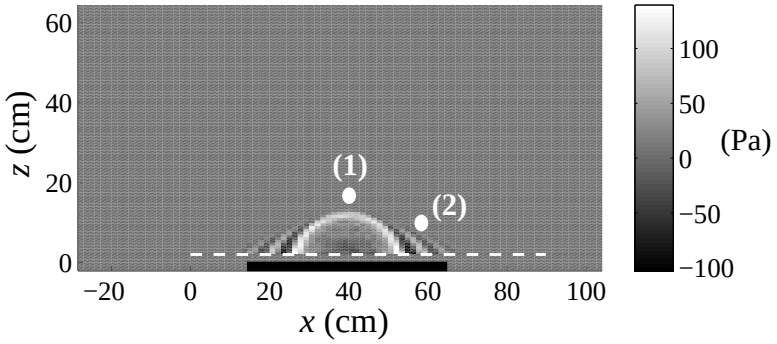

(a) $t = 0.38$ ms

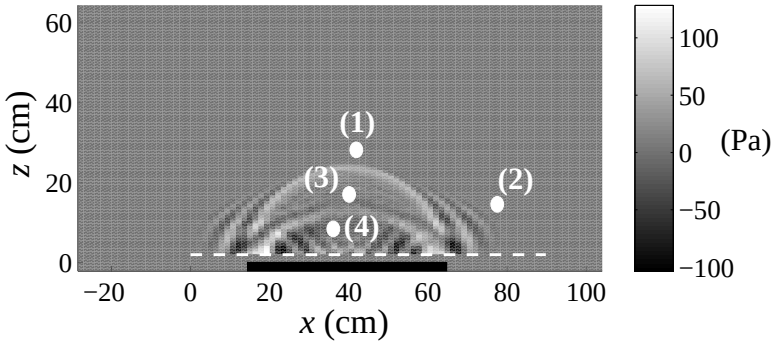

(b) $t = 0.72$ ms

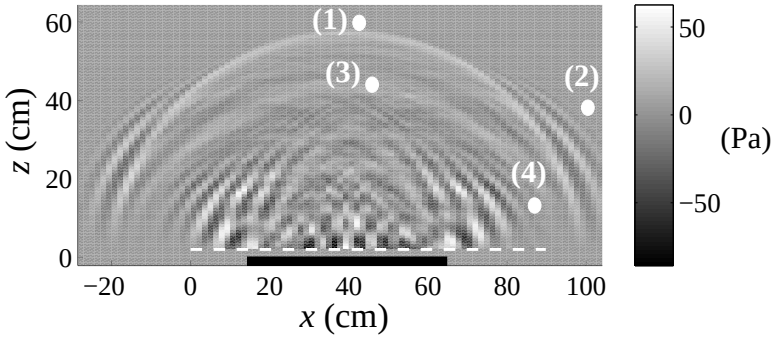

(c) $t = 1.7$ ms

Figure 7. Reconstruction of the sound pressure field in a plane perpendicular to the y-axis. The plate and the hologram locations are respectively illustrated by solid black and dashed white lines.

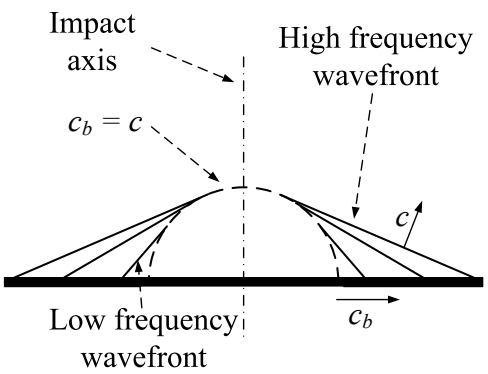

Figure 8. Apparent dispersion phenomenon.

dispersion and radiation due to the flexural waves reflecting on the edges of the plate were clearly visible.

Application of TNAH to backward propagation in order to have a complete reconstruction requires further investigation. Moreover, the radiation due to the reflection of flexural waves on other local changes in the structure's mechanical impedance (holes, added mass, damping treatment, etc.) could also be studied. Such capability would greatly increase our ability to design vibration treatments for impacted structures.

Acknowledgments and notice

This work was supported by the Fonds québécois de la recherche sur la nature et les technologies, the Institut de recherche Robert-Sauvé en santé et en sécurité au travail and the Natural Sciences and Engineering Research Council of Canada. This work was done when J.-F. Blais was affiliated with the École Polytechnique de Montréal.

REFERENCES

[1] S. Schedin, C. Lambourge, and A. Chaigne, Transient sound fields from impacted plates: Comparison between numerical simulations and experiments, *Journal of Sound and Vibration*, 1999, **221**, 471–490.

[2] E. G. Williams, *Fourier Acoustics, Sound Radiation and Nearfield Acoustical Holography*, Academic Press, San Diego, 1999.

[3] J. Adin Mann III, E. G. Williams, K. Washburn, and K. Grosh, Time-domain analysis of the energy exchange between structural vibrations and acoustic radiation using near-field acoustical holography measurements, *The Journal of the Acoustical Society of America*, 1991, **90**, 1656–1664.

[4] J.-F. Blais and A. Ross, Forward projection of transient sound pressure fields radiated by impacted plates using numerical Laplace transform, *The Journal of the Acoustical Society of America*, 2009, **125**, 3120–3128.

[5] D. J. Wilcox, Numerical Laplace transformation and inversion, *International Journal of Electrical Engineering Education*, 1978, **15**, 247–265.

[6] P. Moreno and A. Ramirez, Implementation of the numerical Laplace transform: A review, *IEEE Transactions on Power Delivery*, 2008, **23**, 2599–2609.

[7] L. M. Wedepohl, Power systems transients: Errors incurred in the numerical inversion of the Laplace transform, *Proceedings of Midwest Symposium on Circuits and Systems*, 1983, Puebla, Mexico, 174–178.

[8] A. Ross and G. Ostiguy, Propagation of the initial transient noise from an impacted plate, *Journal of Sound and Vibration*, 2007, **301**, 28–42.